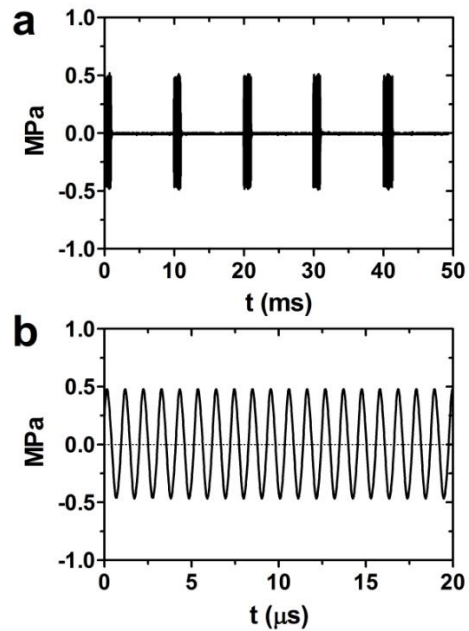


## SUPPLEMENTARY INFORMATION

### 1. Measurement of transmitted ultrasound signal

Consistent ultrasound stimulation within the sonoporation volume was sought in the design of the sonoporation chamber. Hydrophone measurements were made 1-3 mm behind the measured center of the cartridge (50% of vertical width and height) under experimental temperature (37 °C) to characterize the attenuated signal from the therapeutic ultrasound transducer (Figure S1). The pulse repetition frequency (PRF) and pulse duration reported in the article were verified to be 100 Hz and 1 ms, respectively. The peak negative pressure (PNP) was measured to be 0.53 MPa with a calibrated hydrophone. Attenuation from both polystyrene windows and the water volume in the cartridge was measured to be negligible at approximately 2%. Interference relating to reflections into the sonoporation volume were checked by measuring along the edges of the acoustically transparent volume and looking for sudden deviations in ultrasonic amplitude or signal quality.



**Figure S1.** The acoustic driving pulse utilized in all experiments was characterized utilizing a membrane-type needle hydrophone, taken in (a) long and (b) short time increments. Hydrophone measurements showed a 1-ms pulse length, 100-Hz PRF, 1.0-MHz center frequency and  $0.53 \pm 0.03$  MPa PNP at a transducer setting of  $2.0 \text{ W/cm}^2$ , which was used in all sonoporation and transfection experiments.

**Table S1. The effect of sonication and microbubble size on concentration (MB/mL) over time.**

	Time (s)								Half-life
	0		5		30		120		
	Mean	SD	Mean	SD	Mean	SD	Mean	SD	
2- $\mu\text{m}$	$1.0 \times 10^8$	$9.0 \times 10^5$	$3.5 \times 10^7$	$3.5 \times 10^4$	$2.1 \times 10^6$	$2.1 \times 10^4$	$1.5 \times 10^6$	$1.3 \times 10^4$	0.7 s
4- $\mu\text{m}$	$1.1 \times 10^8$	$7.9 \times 10^5$	$3.3 \times 10^7$	$2.1 \times 10^5$	$1.6 \times 10^7$	$7.0 \times 10^4$	$1.1 \times 10^7$	$4.6 \times 10^4$	1.7 s
6- $\mu\text{m}$	$1.1 \times 10^8$	$8.5 \times 10^5$	$9.3 \times 10^7$	$6.1 \times 10^5$	$7.6 \times 10^7$	$4.2 \times 10^5$	$6.5 \times 10^7$	$2.5 \times 10^5$	13.2 s

## 2. Theoretical radial dynamics calculations

The modeling of the radial dynamics of a lipid shell microbubble was performed with MATLAB (Mathworks, Natick, MA, USA) using Marmottant's cavitation model (Marmottant et al. 2005). The effective surface tension of the shell,  $\sigma$ , depends on the bubble radius,  $R$ , and is modeled in three regimes:

$$\sigma(R) = \begin{cases} 0 & \text{if } R \leq R_{buckling} \\ \chi \left( \frac{R^2}{R_{buckling}^2} - 1 \right) & \text{if } R_{buckling} \leq R \leq R_{break-up} \\ \sigma_{water} & \text{if ruptured and } R \geq R_{ruptured} \end{cases} \quad (S1)$$

where  $\chi$  is the elastic modulus and  $\sigma_{water}$  is the surface tension of water. The radial limits for the buckling radius,  $R_{buckling}$ , break-up radius,  $R_{break-up}$ , and ruptured radius,  $R_{ruptured}$ , above are determined by:

$$\begin{aligned} R_{buckling} &= R_0 \\ R_{break-up} &= R_{buckling} \left( 1 + \frac{\sigma_{break-up}}{\chi} \right)^{1/2} \\ R_{ruptured} &= R_{buckling} \left( 1 + \frac{\sigma_{water}}{\chi} \right)^{1/2} \end{aligned} \quad (S2)$$

The internal gas pressure,  $P_g(t)$ , of the lipid shelled bubble is determined by:

$$P_g(t) = P_l(t) + \frac{2\sigma(R)}{R} + 4\mu \frac{\dot{R}}{R} + 4\kappa_s \frac{\dot{R}}{R^2}, \quad (S3)$$

where  $P_l(t)$  is the liquid pressure at the bubble surface,  $\mu$  is the liquid viscosity, and the overdot ( $\dot{\phantom{x}}$ ) denotes a derivative with respect to time,  $t$ . The constant  $\kappa_s$  is the surface dilation viscosity

of the monolayer. For the simulations presented here, the value for  $\sigma_{water}$  is set to 0.0728 N/m and the values for  $\kappa_s$ ,  $\chi$ , and  $\sigma_{break-up}$  are set equal to  $7.2 \times 10^{-9}$  N-s/m, 1 N/m, and 0.13 N/m, respectively, based on the values reported in Marmottant et al. (2005) for the contrast agent BR14.

The radial dynamics of the microbubble are determined by combining the Rayleigh-Plesset equation with the polytropic gas law and the boundary condition (S3):

$$\rho_l \left( R\ddot{R} + \frac{3}{2}\dot{R}^2 \right) = \left[ P_0 + \frac{2\sigma(R_0)}{R_0} \right] \left( \frac{R}{R_0} \right)^{-3\kappa} \left( 1 - \frac{3\kappa}{c} \dot{R} \right) - P_0 - \frac{2\sigma(R)}{R} - \frac{4\mu\dot{R}}{R} - \frac{4\kappa_s\dot{R}}{R^2} - P_{ac}(t). \quad (S4)$$

where  $\mu = 0.001$  Pa-s,  $\rho_l$  is the liquid density (1000 kg/m<sup>3</sup>),  $P_0$  is the hydrostatic pressure (1 atm),  $\kappa$  is the polytropic gas constant for perfluorobutane (1.07) (Morgan et al. 2000),  $c$  is the speed of sound in the liquid (1485 m/s), and  $P_{ac}(t)$  is the acoustic forcing pressure. The acoustic forcing term is modeled as  $P_{ac}(t) = P_a \sin(\omega t)$ , where  $P_a$  is the acoustic pressure amplitude (530 kPa) and  $\omega = 2\pi f$  is the angular frequency corresponding to the transducer frequency,  $f = 1$  MHz. Simulations were conducted for bubbles with initial diameters of 2, 4 and 6  $\mu\text{m}$  for 10 acoustic cycles. The radius was nondimensionalized as:

$$R^* = \frac{R}{R_0} \quad (S5)$$

### 3. Flow cytometric analysis

The determination of optimal flow rates, cut-offs, compensation and gating were performed through the Accuri C5 and C6 software. The forward-scatter-H cutoff value for measured samples was  $8 \times 10^5$ , with the upper limit being  $10^{7.2}$ . Gating was conducted as described in Figure S2. Compensation of FL1-A (520 nm) and FL2-A (560nm) were conducted with both FITC dextran and EGFP in relation to ethidium homodimer-1 as detailed by the CU Denver Cancer Center flow cytometry core. A slight undercompensation on FL2-FL1 (<0.2%) was noted but signals from the live-treated and dead cell groups were considered to be strong and distinct when compared to the controls, with minimal gate contamination from autofluorescent cells. Fluorescence microscopy (Olympus IX71) with a 480/520 nm excitation/emission was conducted to visualize internalization of FITC-dextran in sonoporated (permeabilized and viable) cells, and to confirm that no residual FITC remained on the surface of the cells (Fig. S3)

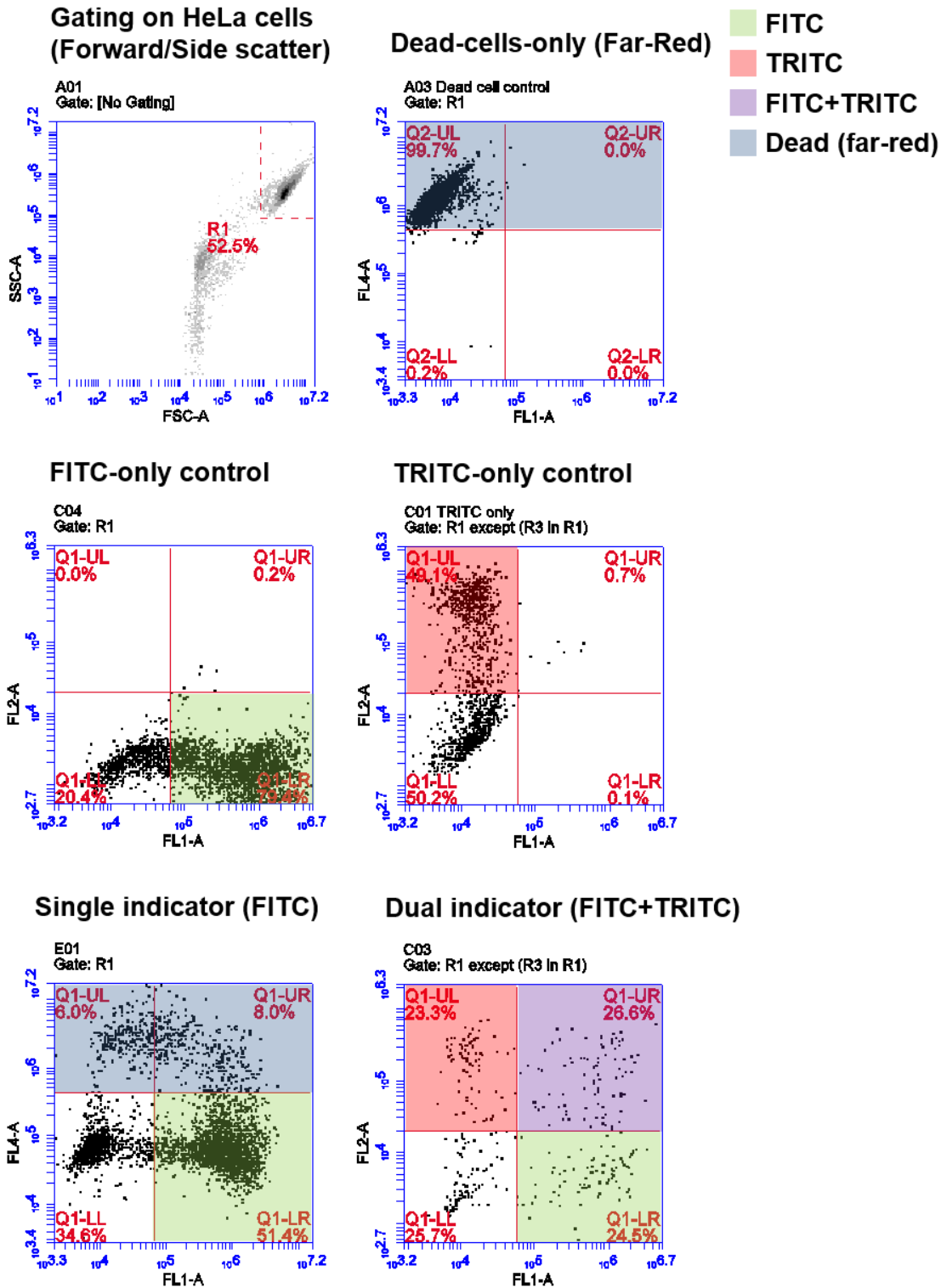


**Figure S2.** Flow cytometry gating for single- and dual-indicator studies. Fluorescence compensation was performed using controls for FITC/far-red (0% spectral overlap), and between FITC-TRITC (27.1% overlap). Cell samples were gated using scatter, and fluorescent cells were detected using three channels for FITC (FL1A), TRITC( FL2A) and far-red lysine-binding dye (dead cells, FL4A).

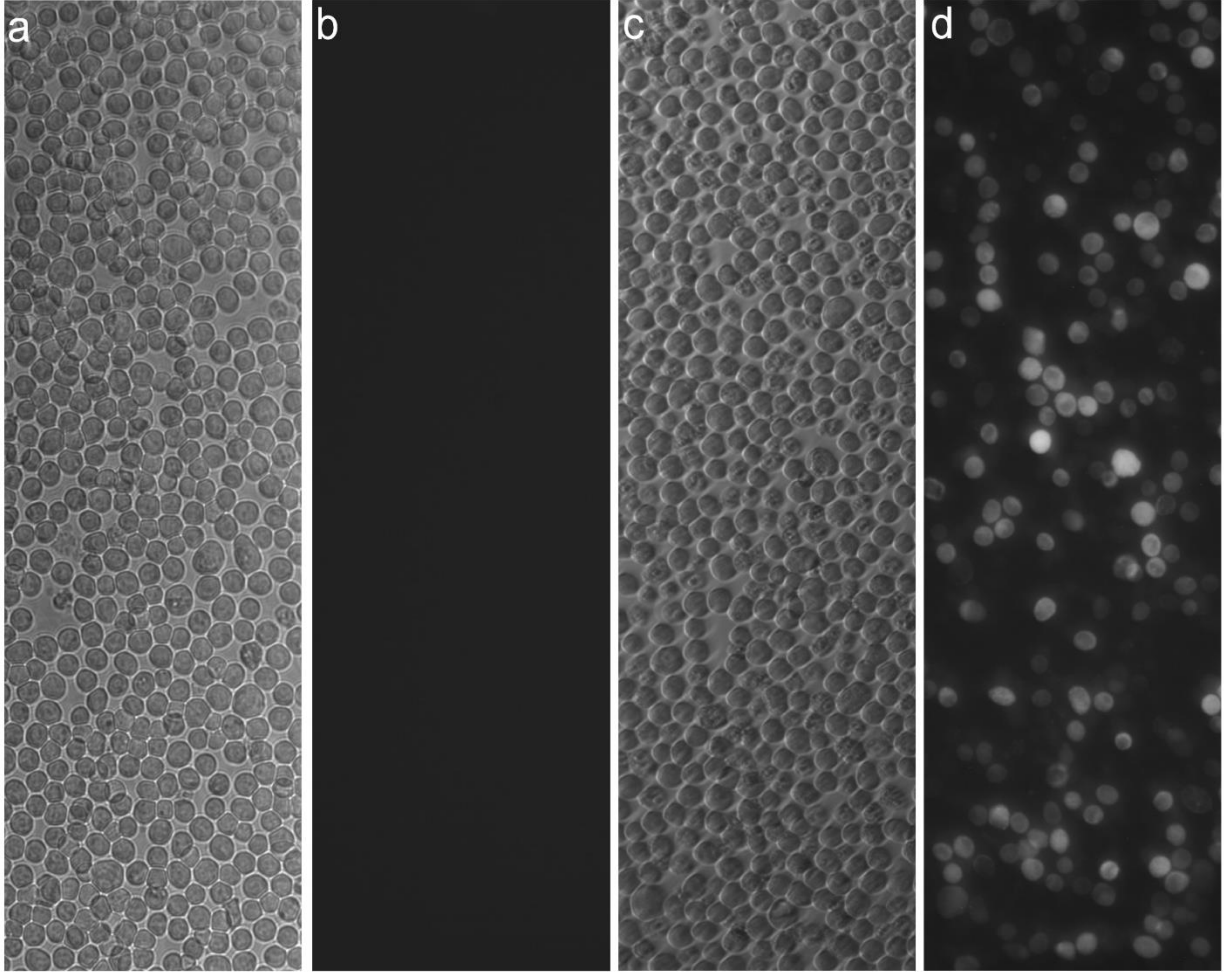


**Figure S3.** Microscopy images of free/suspended control and sonoporated HeLa cells post-processed with anti-fluorescein were captured using an Olympus IX71 inverted microscope with a 20x objective. (a, b) Bright-field and fluorescence images of control cells treated with FITC-dextran and ultrasound, but not microbubbles. (c, d) Bright-field and fluorescence images of cells sonoporated with ultrasound, microbubbles and FITC-dextran. Note the cell-to-cell variation in fluorescence intensity seen in (d).

#### 4. Predictions of sonoporated fractions

Predictions were made on the multiplicative effects of sequential sonoporations using the following system of equations. The fractions of treated ( $\chi_T$ ), dead ( $\chi_D$ ) and lysed ( $\chi_L$ ) cells after the first sonoporation were determined based on data from a prior study with single sonoporation under similar conditions [36], and their values were held constant to predict the effects from subsequent (second, third and fourth) sonoporations. The total number of initial cells ( $N_0$ ) contained a small fraction ( $\chi_{D,0} = 3\%$ ) of dead cells owing to trypsinization, resuspension and handling. Thus, the initial number of dead cells was given as:

$$N_{D0} = \chi_{D,0}N_0 \quad (\text{S6})$$

The remaining cells prior to sonoporation were therefore “untreated” cells (i.e., viable and non-fluorescent):

$$N_{U,0} = (1 - \chi_{D,0})N_0 \quad (\text{S7})$$

The initial number of treated ( $N_{T,i}$ ) and lysed ( $N_{U,0}$ ) cells was zero. Following each sonoporation, the total number of cells ( $N_i$ ) declines owing to lysis:

$$N_i = N_0(1 - \chi_L)^i \quad (\text{S8})$$

where index  $i$  is the sonoporation number and  $\chi_{L}$  is the fraction of cells lysed in each sonoporation step ( $\chi_{L} = 3\%$ ). The number of lysed cells increases with each sonoporation:

$$N_{L,i} = N_0 - N_i \quad (\text{S9})$$

The number of dead cells following the  $i$  sonoporation step ( $N_{D,i}$ ) is given by:

$$N_{D,i} = (1 - \chi_{L})(N_{D,i-1} + \chi_D N_i) \quad (\text{S10})$$

where  $\chi_D$  is the fraction of cells killed in each sonoporation step ( $\chi_D = 7\%$ ). Therefore, the number of treated ( $N_{T,i}$ ) and untreated ( $N_{U,i}$ ) cells following the  $i$  sonoporation step are given by:

$$N_{T,i} = (1 - \chi_L - \chi_D)(N_{T,i-1} + \chi_T N_{U,i-1}) \quad (\text{S11})$$

$$N_{U,i} = N_i - N_{L,i} - N_{D,i} - N_{T,i} \quad (\text{S12})$$

where  $\chi_T$  is the fraction of cells treated (viable and fluorescent) produced in each sonoporation step ( $\chi_T = 49\%$ ). Equations 1-7 were iterated with each sonoporation step ( $i = 1$  to 4) to predict the numbers of treated, dead, lysed and untreated cells (Fig. S4). These simple model predictions were then compared to experimental results using the methods discussed below.

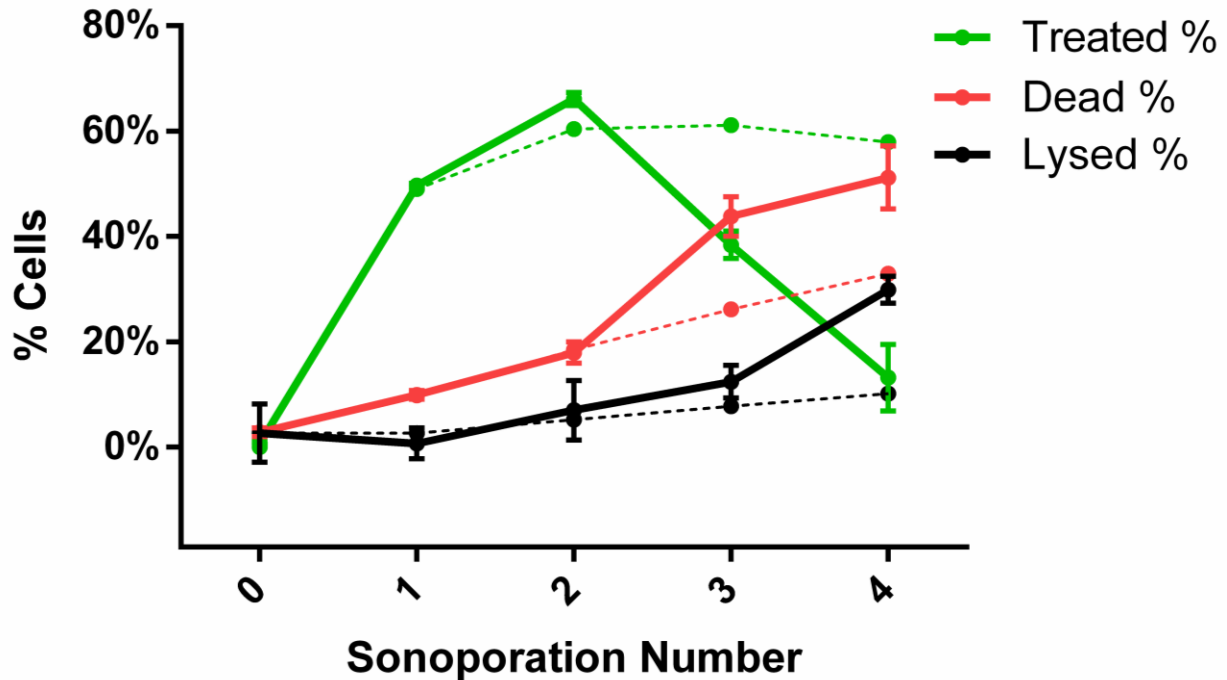


**Figure S4.** A comparison of predicted (dotted) and experimentally derived (solid lines) treated cells (green), cell death (red) and lysis (black lines). See the Theory section above for equations and values used to calculate the predicted lines.

### 5. Comparison of transfection efficiencies

Plasmid EGFP-C3 (Clontech, Mountain View, CA, USA) was used for transfection assays of HeLa cells in suspension (ATCC, Manassas, VA, USA). Electroporation was conducted with an IBI Gene Zapper 450/2200 (IBI, New Haven, CT) on cells in suspension ( $1-3 \times 10^6$  cells/200  $\mu$ L with 5  $\mu$ g DNA) at a voltage of 0.22 kV and capacitance at 500  $\mu$ F. Microbubble-treated samples were sonoporated with 2- and 6- $\mu$ m microbubbles at  $10^8$  MB/mL in a 200  $\mu$ L volume with 5  $\mu$ g of DNA for 2 minutes at 2 W/cm<sup>2</sup>, 10% DC with a Dynatron® 125 (Dynatronics, Salt Lake City, Utah). HeLa cells from both electroporation and sonoporation were cultured for 24 hr before the addition of ethidium homodimer-1 (Invitrogen, NY, USA) to stain for dead cells. Flow-cytometric analysis was conducted to determine EGFP-expressing and dead cells.

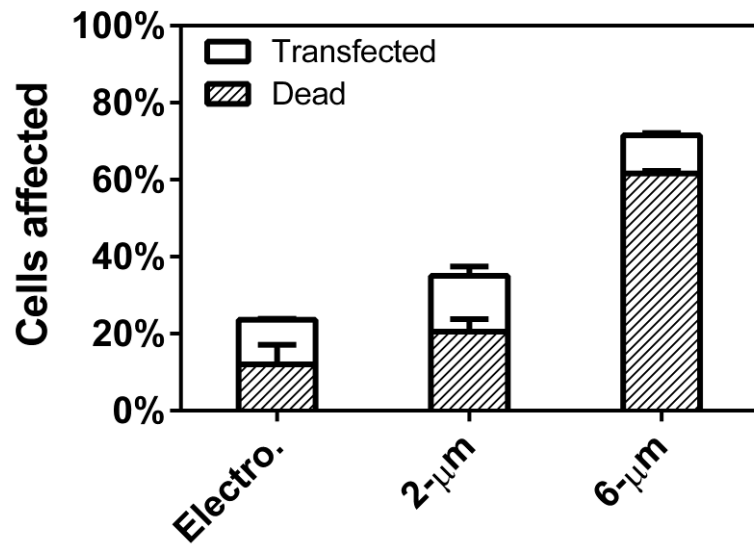


**Figure S5.** A comparison of CMV-EGFP-plasmid transfection efficiencies between electroporation, 2- and 6-μm unmixed microbubble sonoporation of HeLa cells.